

## Smart Nonaqueous Foams from Lipid-Based Oleogel

Anne-Laure Fameau,<sup>\*,†</sup> Stephanie Lam,<sup>‡</sup> Audrey Arnould,<sup>†</sup> Cédric Gaillard,<sup>†</sup> Orlin D. Velev,<sup>‡</sup> and Arnaud Saint-Jalmes<sup>\*,§</sup>

<sup>†</sup>Biopolymères Interactions Assemblages, INRA, Rue de la Géraudière, 44316 Nantes, France

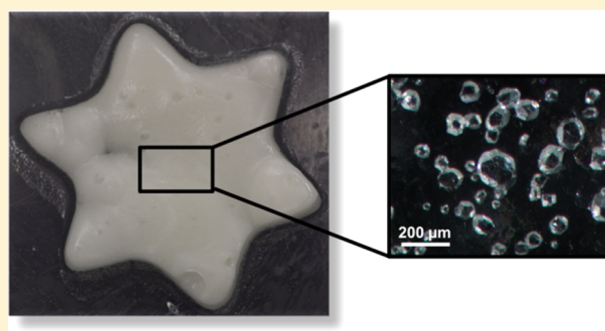
<sup>‡</sup>Department of Chemical and Biomolecular Engineering, North Carolina State University, Raleigh, North Carolina 27695, United States

<sup>§</sup>Institut de Physique de Rennes, UMR CNRS 6251-Université Rennes 1, 35000 Rennes, France

### Supporting Information

**ABSTRACT:** Oil foams are composed of gas bubbles dispersed in an oil phase. These systems are scarcely studied despite their great potential in diverse fields such as the food and cosmetic industries. Contrary to aqueous foams, the production of oil foams is difficult to achieve due to the inefficiency of surfactant adsorption at oil–air interfaces. Herein, we report a simple way to produce oil foams from oleogels, whose liquid phase is a mixture of sunflower oil and fatty alcohols. The temperature at which the oleogel formed was found to depend on both fatty alcohol chain length and concentration. The air bubbles in the oleogel foam were stabilized by fatty alcohol crystals. Below the melting temperature of the crystals, oleogel foams were stable for months.

Upon heating, these ultrastable foams collapsed within a few minutes due to the melting of the crystal particles. The transition between crystal formation and melting was reversible, leading to thermoresponsive nonaqueous foams. The reversible switching between ultrastable and unstable foam depended solely on the temperature of the system. We demonstrate that these oleogel foams can be made to be photoresponsive by using internal heat sources such as carbon black particles, which can absorb UV light and dissipate the absorbed energy as heat. This simple approach for the formulation of responsive oil foams could be easily extended to other oleogel systems and could find a broad range of applications due to the availability of the components in large quantities and at low cost.



## INTRODUCTION

The most common types of foams are the aqueous systems formed by gas bubbles dispersed in an aqueous phase.<sup>1</sup> They have been widely studied and can be found in a wide variety of applications such as detergency, food, cosmetic products, and so forth.<sup>2</sup> Aqueous foams are thermodynamically metastable systems. Their production and stabilization requires the use of stabilizing agents, which can be surfactant molecules, polymers, proteins, or particles dispersed in the aqueous phase.<sup>2,3</sup> The role of these components is to prolong the stability of the foam by slowing down the three main mechanisms of foam decay: drainage, coarsening, and coalescence.<sup>1</sup> The control of foam stability is a major challenge in foam science, and recent research progress has resulted in the creation of ultrastable aqueous foams as well as new categories of responsive foams.<sup>4–11</sup> The stability of stimuli-responsive foams can be tuned between stable and unstable states either by changes in solution conditions (pH, temperature and ionic strength) or with the application of an external field (light and magnetic field).<sup>9</sup> Until now, only four examples based on surfactants have shown a reversible transition between stable and unstable states using light, temperature, or gas.<sup>12–16</sup>

Contrary to aqueous foams, few studies have been devoted to the understanding of oil foams, composed of gas bubbles dispersed in an oil phase, despite their occurrence in various fields and their economic consequences such as in the petroleum industry.<sup>17</sup> To our knowledge, no report of responsive oil foams is available in the literature. In aqueous foams, the main feature of the stabilizing component is to adsorb at the air–water interface reducing the relatively high water–air interfacial tension ( $\approx 72 \text{ mN}\cdot\text{m}^{-1}$  at  $25^\circ\text{C}$ ) to values in the range of  $20\text{--}40 \text{ mN}\cdot\text{m}^{-1}$ . In the case of nonpolar oils, the tension at the oil–air interface is already low ( $20\text{--}25 \text{ mN}\cdot\text{m}^{-1}$ ), making the adsorption of oil-soluble surfactants at the interface energetically unfavorable. This makes the production of oil foams using traditional surfactants challenging. However, oil foams (with limited stability) can be produced using fluorocarbon-based surfactants, poly(alkene)s, or a liquid crystal dispersion.<sup>18–21</sup> As in the case of aqueous foams, particles can also give rise to stable oil foams. In these systems, particles form a close-packed layer around air bubbles to

**Received:** October 2, 2015

**Revised:** November 16, 2015

**Published:** November 25, 2015

prevent coalescence and coarsening. The adsorption of particles at an air/liquid surface depends on the contact angle the particles form with the air–liquid interface measured through the liquid phase.<sup>22</sup> Particles can be made to be partially oleophobic through functionalization with fluoro groups and used to make Pickering oil foams.<sup>23–26</sup>

Another way to stabilize oil foams by Pickering mechanisms is through the use of monoglycerol or diglycerol fatty acid esters, which can form crystalline particles in oil. Such particles have been shown to stabilize foams by forming a robust coating on the surface of air bubbles to arrest diffusion.<sup>27–31</sup> Studies have shown that foam stability increases with monoglyceride/diglyceride (hydrocarbon) chain length.<sup>27,28</sup> For example, foam stability at 25 °C was on the order of minutes for systems stabilized by glycerol monocaprylin (11 carbons) and hours for systems stabilized by glycerol monocaprin (13 carbons). The effect of stabilizer concentration on foam stability has also been reported.<sup>29,30</sup> In the case of the diglycerol monomyristate, foam from olive oil containing 1 wt % diglycerol monomyristate was stable for ~20 min, whereas foam containing 10 wt % diglycerol monomyristate was stable for more than one month at 25 °C.<sup>30</sup> It has been demonstrated that monoglycerides and diglycerides can lead to the formation of oleogels due to their ability to form crystals in edible oils.<sup>32–34</sup> In these oleogels, it is known that both the fatty acid ester concentration and hydrocarbon chain length affect the temperature at which crystal formation occurs and, consequently, control the gelation process.<sup>32–34</sup> By considering the results obtained for oil foams and oleogels in similar systems, some questions arise concerning the mechanisms of foam stabilization by monoglyceride and diglyceride particles. All systems previously reported in the literature were studied at the same temperature (25 °C). However, temperature seems to have a drastic effect on the formation of particles in oil as highlighted in previous oleogel studies.<sup>35</sup> Thus, the effect of temperature on foam stability in these oil foam systems has yet to be understood and utilized.

The goal of this study is to elucidate the link between oil foam stability and temperature for oleogel systems in order to control and tune the dispersion stability using external stimuli. We chose as a model oleogel system fatty alcohols dispersed in sunflower oil. All oleogel components are available in large quantities at low cost and are already widely used for applications in the cosmetics industry. Fatty alcohols are known to be capable of gelling oils by forming crystal platelets.<sup>36–38</sup> However, few reports containing quantitative data are available for these systems.<sup>37–39</sup> Here we used our study on oil foams to also obtain information on the physicochemical properties of oleogels derived from fatty alcohols, which could be very useful from both the fundamental and applied perspectives in the oleogel field.<sup>40</sup> We varied the chain length of the fatty alcohols from 14 to 18 carbons and their concentration from 1 to 20% (w/w). Oleogel properties were characterized using differential scanning calorimetry (DSC), wide-angle X-ray scattering (WAXS), rheology, and microscopy. The crystallization and the melting temperatures of the oleogels were precisely determined as a function of both hydrocarbon chain length and fatty alcohol concentration. Next, foams were produced and their stability was studied as a function of temperature.

We clearly demonstrate that the stability of foams produced from oleogels is directly linked to hydrocarbon chain length and fatty alcohol concentration, both of which affect the formation and melting of the crystal particles. Below the

melting temperature of the crystals, all foams were stable for months regardless of the fatty alcohol chain length and concentration. Above the melting temperature of the crystals, no foams could be produced. The melting of the crystals was found to be a phenomenon spanning a wide range of temperatures leading to a progressive decrease in the quantity of particles in the foam during the melting transition. Therefore, foam stability decreases gradually with increasing temperature until the melting process is completed. It was also noted that the stability of oleogel foams could be easily tuned by changing temperature. In view of the strong effect of temperature on foam stability, we demonstrate how an approach used to develop multiresponsive aqueous foams based on surfactants can be easily extended to these oil foams to demonstrate, for the first time, responsive foams from nonaqueous systems.

## RESULTS AND DISCUSSION

**Oleogel Formation and Characterization.** Oleogels were prepared by mixing fatty alcohols (FAOH) and sunflower oil. We characterized the crystallization and melting of oleogels at different formulations, which serve as a basis for oil foam preparation. We varied both the FAOH concentration and chain length. For the sake of clarity, we designate the FAOH as a function of alkyl chain length: C14OH (1-tetradecanol), C16OH (1-hexadecanol), and C18OH (1-octadecanol). All samples stored at high temperatures were in the liquid state and flowed freely when sample tubes were inverted (Figure 1). Upon cooling, the samples could be turned upside down without inducing any flow under gravity due to oleogel formation.

To obtain qualitative information about the microstructure of the oleogels, samples were viewed using polarized light microscopy. A typical micrograph is shown in Figure 1. For all samples, gelation occurred due to the formation of large

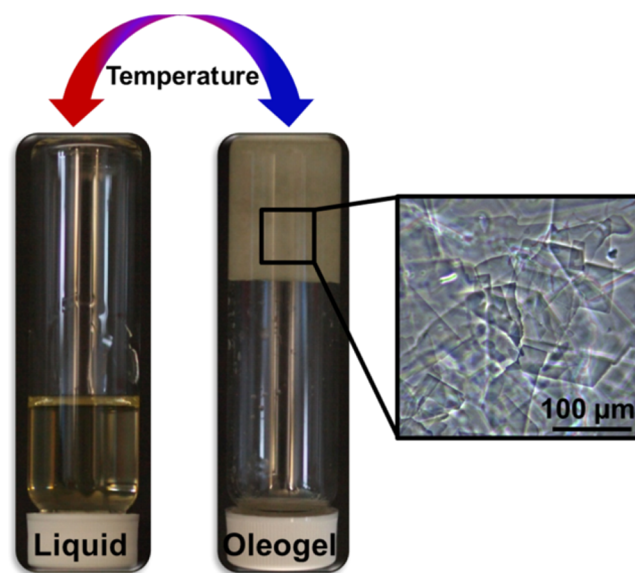


**Figure 1.** Photographs of an oleogel containing 10 wt % C18OH showing the liquid state of the sample above 50 °C (left) and oleogel formation below 30 °C (right). The sample is liquidlike at  $T > T_m$  offset and forms a gel at  $T < T_c$  offset. The micrograph of the oleogel obtained by phase contrast microscopy shows the platelet morphology of the crystals.

solid crystals with a platelet-like structure. The length and width of the crystals were on the order of 50–200  $\mu\text{m}$ .

The temperature at which the sample begins to transit from an oleogel to a liquid is called the onset of melting ( $T_m$  onset) and the end of this process corresponds to the offset of melting ( $T_m$  offset) (Figure 2a). The temperature at which crystal

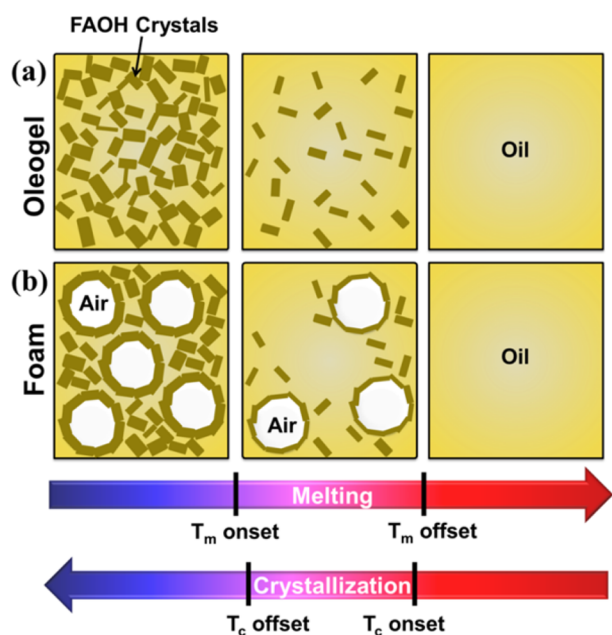


**Figure 2.** (a) Schematic illustrating that fatty alcohol crystal formation begins at  $T_c$  onset and ends at  $T_c$  offset. The oleogel begins to transit from the solid to liquid state due to crystals melting at  $T_m$  onset. At  $T > T_m$  offset, FAOH crystals are no longer present in the mixture, which is now fully in the liquid state. (b) Schematic illustrating foam stabilization due to the presence of FAOH crystals at the oil–air interface below  $T_c$  onset. By increasing temperature to  $T > T_m$  onset, FAOH crystals located in the bulk as well at the interface melt, resulting in foam destabilization.

formation begins to occur, leading to the oleogel state, is referred to as the onset of crystallization ( $T_c$  onset); and the temperature corresponding to the end of this process, the offset of crystallization ( $T_c$  offset).

Differential scanning calorimetry (DSC) was used to precisely determine all temperatures as well as the enthalpies associated with the phase transitions for different oleogel compositions. We measured the enthalpograms for all systems as a function of FAOH concentration. All the DSC heating and cooling enthalpograms can be found in Figure 3 and numerical data are listed in Tables S1–3. Upon cooling, only one sharp exothermic peak was observed for all samples tested, corresponding to the crystallization process (Figure 3a–c). One single broad endothermic peak was observed upon heating (Figure 3d–f). This peak corresponds to a first order endothermic transition typical of melting processes. The evolution of the enthalpies as a function of FAOH concentration is presented in Figure S1. Both the enthalpy of melting and enthalpy of crystallization increased linearly with FAOH concentration.

In Figure S2, we show the onset and offset of  $T_m$  and  $T_c$ , which correspond to the beginning and end of oleogel melting and crystallization transition, respectively. For all samples, the temperature difference between the beginning ( $T_{\text{onset}}$ ) and the

end ( $T_{\text{offset}}$ ) of the transition processes was around 5 and 25  $^{\circ}\text{C}$  for crystallization and melting, respectively. The crystallization process occurs within a narrow temperature range whereas the melting process spans a wide range of temperatures. By increasing the FAOH chain length, all the melting and crystallization temperatures were shifted toward higher values reaching almost a constant value at a FAOH concentration of 18% (w/w) in the oleogel. The melting and crystallization process can be tuned from 5 to 50  $^{\circ}\text{C}$  by modifying FAOH concentration and chain length.

To characterize the structure of the crystals at the molecular scale, we performed Wide-Angle X-ray Scattering (WAXS) measurements below  $T_m$  onset. The WAXS spectra for the different FAOH at various concentrations are presented in Figures 4 and S3–5. In all WAXS spectra, two major peaks were observed at 1.51 and 1.7  $\text{\AA}^{-1}$ , corresponding to characteristic lengths of 3.7 and 4.15  $\text{\AA}$  in real space. These peaks are the signatures of the solid state of the fatty alcohol, which arises from the crystalline structure of the hydrophobic tail. They are characteristic of  $\beta$  phase crystals which are composed of orthorhombically arranged fatty alcohol molecules.<sup>33,38</sup> For  $T > T_m$  offset, no peak was observed in the WAXS spectra since all crystals melted and all samples were in the liquid state.

To complete the previous studies, we also investigated the rheological properties of the oleogels as a function of temperature at various FAOH concentrations and chain lengths. We focused on the evolution of the elastic and viscous moduli,  $G'$  and  $G''$ , respectively, monitored at a low and constant amplitude of deformation and frequency during both cooling and heating ramps. In Figure 5a, we show a typical data set for C18OH at 8 wt %. During the cooling process, for  $T > T_c$  onset, the values of  $G'$  and  $G''$  were low (around  $10^{-1}$  Pa) and  $G'' > G'$  corresponding to viscous (liquid-like) samples. It is important to notice that for such low deformations and as the oil viscosity remains low (50 mPa·s), the rheological measurements are within the limit of low torques ( $<1 \mu\text{N}\cdot\text{m}$ ). During sample cooling, the viscous and elastic moduli displayed an abrupt change as a function of temperature, corresponding to the transition between the liquid and the oleogel states. The temperature at which this phenomenon was detected is the same as  $T_c$  onset determined using DSC. For  $T < T_c$  offset, the values of  $G'$  and  $G''$  were high (around  $10^5$  Pa), and  $G' > G''$  corresponding to an elastic (solidlike) behavior. This abrupt change in sample response to the applied deformation can be interpreted as the macroscopic result of FAOH crystallization. The occurrence of solid crystals percolating through the sample gives rise to an elastic, gel-like structure. Sample transition between viscous and elastic response occurred within a few degrees. Below  $T_c$  offset, the elastic moduli reached a maximum value of  $G'_{\text{max}}$ .

Upon heating, both the viscous and elastic moduli decreased gradually with temperature until a sharp decrease was observed (Figure 5). The temperature at which the moduli began to decrease was around  $T_m$  onset as determined using DSC. For  $T < T_m$  onset, we observed  $G' > G''$  with values on the order of  $10^5$ – $10^6$  Pa. At  $T > T_m$ , the gradual decrease in both  $G'$  and  $G''$  comes from the melting of the FAOH crystals. At the end of melting process,  $G'' > G'$  with values around  $10^{-1}$ – $10^{-2}$  Pa. The end of the melting process corresponds with the end of the sharp decrease in moduli vs temperature, and occurred around  $T_m$  offset as determined by DSC. All these rheological measurements were consistent with DSC results, confirming

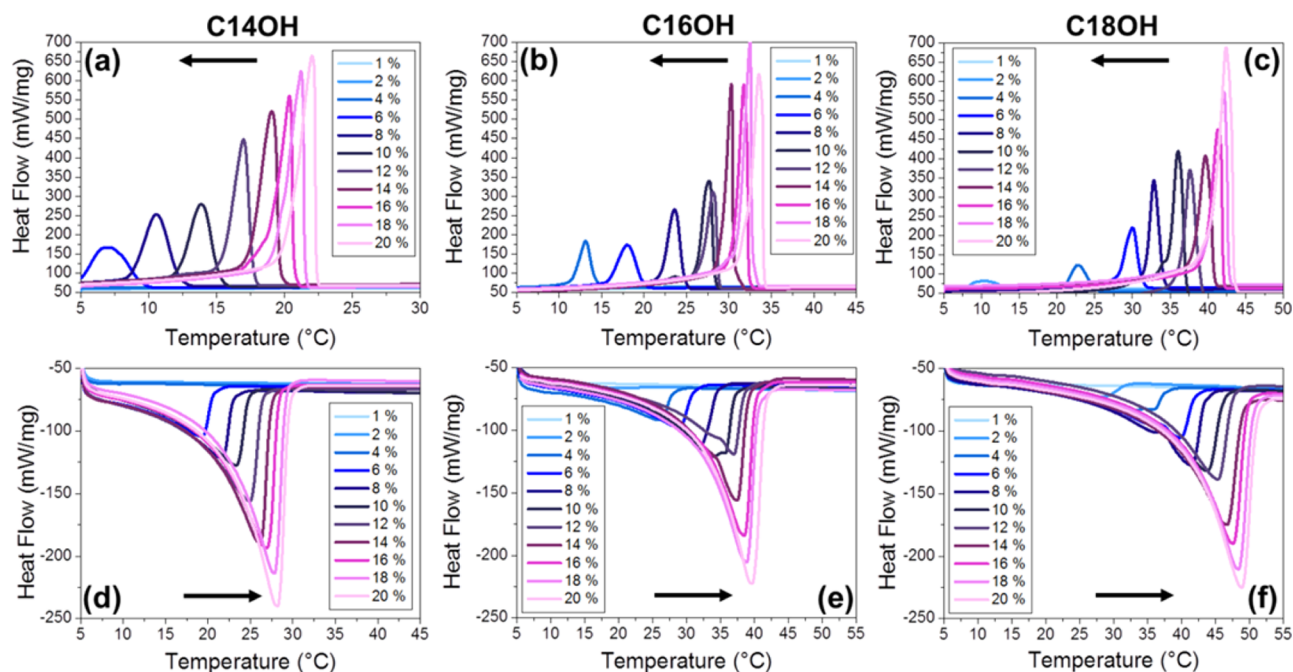


**Figure 3.** Heat flow curves as a function of FAOH concentration for C14OH (a, d), C16OH (b, e), and C18OH (c, f) upon cooling (a–c) and upon heating (d–f). Upon cooling, one sharp exothermic peak, corresponding to the crystallization process, was observed. Upon heating, one single broad endothermic peak, typical of a melting process, was observed.

that the crystallization process occurs within a narrow temperature range ( $\Delta T \sim 5^\circ\text{C}$ ), whereas the melting process spans a wide range of temperatures ( $\Delta T \sim 25^\circ\text{C}$ ). By increasing the concentration of C18OH, we observed an increase in dynamic moduli and the temperatures linked to the melting and crystallization processes were also shifted to higher temperatures in accordance with DSC results (Figure S6a).

Another parameter that plays an important role in the crystallization and melting process of the oleogels is the FAOH chain length. In Figure 5, we compare the rheological behavior of C14OH and C18OH at the same concentration (8 wt %). For C14OH, a sharp transition on cooling and a wider one on heating was observed, which was associated with well-defined crystallization and melting temperatures (Figure 5b). The same behavior as previously described for C18OH was observed. All the transitions (melting and crystallization) were shifted to lower temperatures in the C14OH samples in comparison with oleogels containing C18OH at the same concentration. As already observed by DSC measurements, by decreasing the FAOH chain length, we can shift the transition temperatures of the oleogels to lower values. For the C14 and C18 FAOHs,  $G'_{\text{max}}$  at  $T = 15^\circ\text{C}$  was around  $5 \times 10^4$  Pa. Thus, the difference in chain length between C14OH and C18OH did not result in a change in  $G'_{\text{max}}$  for oleogels containing 8 wt % of the FAOHs. This means that the elasticity of the oleogel is mainly dictated by FAOH concentration rather than chain length.

Amplitude and frequency sweep experiments were performed for oleogels containing 16 wt % C18OH at  $20^\circ\text{C}$  so that the sample was in the oleogel state (Figure S6b, c). No signs of yielding were observed in the samples when the amplitude was increased from 0.1% up to 25%, and frequency was varied from 0.1 to 5 Hz. In addition,  $G'$  was always higher than  $G''$  indicating that the sample remained a gel under the range of test conditions applied. From these experiments, we conclude

that high deformations or frequencies are necessary to induce irreversible flow within the oleogel.

**Foam Properties.** In addition to characterizing oleogel properties as a function of temperature, we investigated their foaming properties as well. For temperatures above  $T_m$  offset, stable foam could not be produced due to the absence of crystal particles. For  $T < T_c$  offset, it was impossible to incorporate bubbles inside the oleogel using our homogenization process (Figure S7). Therefore, foams were produced by aerating the oleogel while simultaneously inducing FAOH crystallization by placing the liquid samples inside an ice bath. This procedure led to the formation of white creamy foam. The temperature of the foam immediately after production was around  $10^\circ\text{C}$ . These nonaqueous foams were composed of relatively small, non-spherical bubbles (mean diameter  $< 200\ \mu\text{m}$ ) possessing textured surfaces (Figure 6). Each foam bubble was covered by adsorbed fat crystals which prevented the relaxation of the bubble to a spherical shape.<sup>41</sup> The foams produced from the three different FAOH had similar structure (Figures S8 and 9). We recorded the scattering spectra of the foam by WAXS to determine the structure of the crystals inside the foam. Major peaks were observed at  $1.52$  and  $1.73\ \text{\AA}^{-1}$  as in the nonaerated oleogels, confirming that the crystal structure of the particles inside the foam is the same as that in the original oleogel (Figure S10). These foams were ultrastable due to both the adsorption of FAOH crystals to the air–oil interface as well as their structuring in the continuous phase (Figure 2b).

We measured foam overrun as a function of FAOH concentration for C14OH, C16OH, and C18OH (Figure 7 and Table S4). The overrun increased with increasing alkyl chain length and fatty alcohol concentration. The maximum overrun observed was 75% for oleogel containing C18OH at 10 wt %. At constant FAOH chain length, the increase in overrun as a function of FAOH concentration can be explained by an increase in the volume fraction of crystal particles present to stabilize air bubbles. The increase in overrun observed with

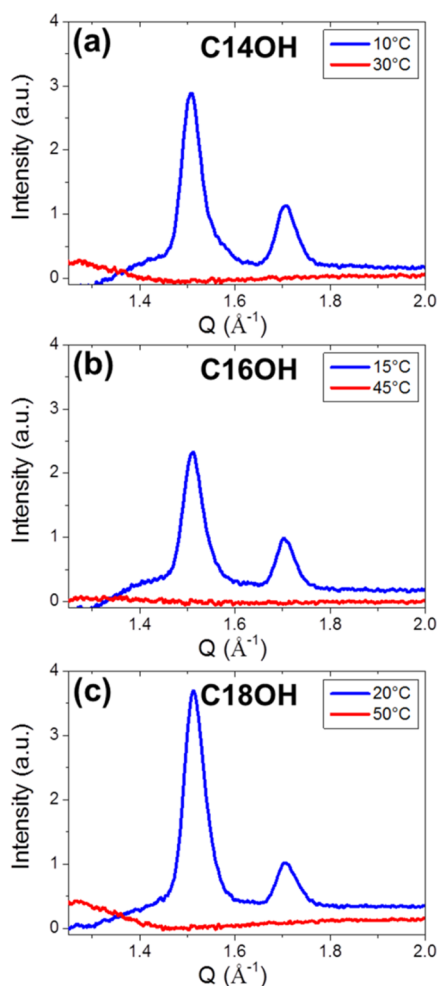


**Figure 4.** WAXS spectra measured below  $T_m$  onset (blue curves) and above  $T_m$  offset (red curves) determined by DSC for (a) C14OH at 10 wt %, (b) C16OH at 10 wt %, and (c) C18OH at 10 wt %. Spectra were recorded after 30 min equilibration at the measurement temperature.

increasing alkyl chain length can be related to the  $T_c$  onset of the crystals forming the oleogel. A higher crystallization temperature results in crystal formation earlier during the foaming process, leading to higher overrun.

For all samples, foam stability with time was studied below  $T_m$  onset where the foam volume remained stable for months

(Figure 6). No drainage and no changes in bubble size were detected. Additionally, when the foam was turned upside down, no flow was observed. The oil foam was in a gelled state (Figure S11).

We studied the rheological properties of these ultrastable oil foams by performing oscillatory measurements at 20 °C ( $T < T_m$  onset for all the foams). In Figure 8a and b, the results of strain sweeps (at a fixed frequency  $f = 1$  Hz) for C18OH at 12 and 16 wt % are presented. There is a range of low amplitude ( $\gamma$ ) where  $G' > G''$ , followed by a regime where  $G'' > G'$  at higher  $\gamma$ . The shape of the curves and the balance between the two moduli show a jammed and glassy state at low  $\gamma$ , followed by viscous flow above a yield point. This rheological behavior is already known and described in the literature for aqueous foam systems.<sup>42</sup> The yield strain (defined here when  $G' \sim G''$ ) was shifted to higher  $\gamma$  by increasing the C18OH concentration in the foam. In contrary to the pure oleogels, which showed no yielding even at high deformations, it was easier to induce an internal flow once gas was incorporated inside the oleogel. The elastic moduli for the oil foams were of the order of  $10^3$ – $10^4$  Pa at low strain deformation. For the pure oleogel, the elastic moduli were around  $10^5$ – $10^6$  Pa. Thus, the ranges of  $G'$  and  $G''$  decreased from the values found for the pure oleogels. The process of gas incorporation could also fracture the crystal platelets. Smaller platelet sizes could lead to less percolation in the bulk, and, as when the amount of FAOH is reduced, to lower elastic moduli. Therefore, the easy yielding of the foams made from oleogels is probably due mainly to the presence of air bubbles and to crystals/platelets of smaller sizes. Incorporating an air phase during crystallization strongly modified the rheological properties of the oleogel. This shifted the system from a strong solid-like gel, preferring to slip at walls than to be sheared in bulk, to a soft elastic material, holding its shape at low deformations, but easily yielding under shear. Together with the temperature and the amount of FAOH, the incorporation of a gas phase turns out to be another way to adjust the viscoelasticity of the material.

In Figure 8c and d, the results of frequency sweeps (at a fixed amplitude  $\gamma = 1\%$ ) for 12 and 16 wt % C18OH are presented. At the lowest frequencies, the foam rheological behavior shifted from an elastic to a viscous behavior. This change implies that an internal mode of relaxation was able to relax the stress and unjam the FAOH platelets on long time scales ( $t > 100$  s). This behavior is also linked to the size of the platelets since local rearrangements are easier for smaller sized platelets.

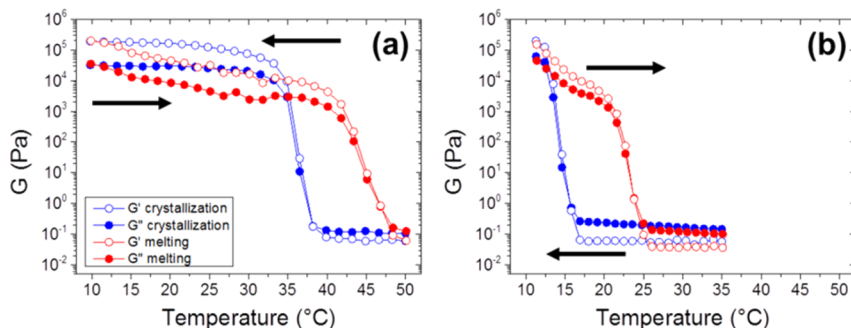


**Figure 5.** Variations of  $G'$  (○) and  $G''$  (●) upon heating (red symbols) correspond to melting, and upon cooling (blue symbols) correspond to crystallization. Above the melting temperature of the fatty alcohol,  $G'' > G'$ , which denotes a liquidlike system. Below the crystallization temperature of the fatty alcohol,  $G' > G''$ , demonstrating that the system is more solidlike. (a) Oleogel containing 8 wt % C18OH and (b) 8 wt % C14OH. The moduli were measured at  $f = 1$  Hz and  $\gamma = 1\%$ .

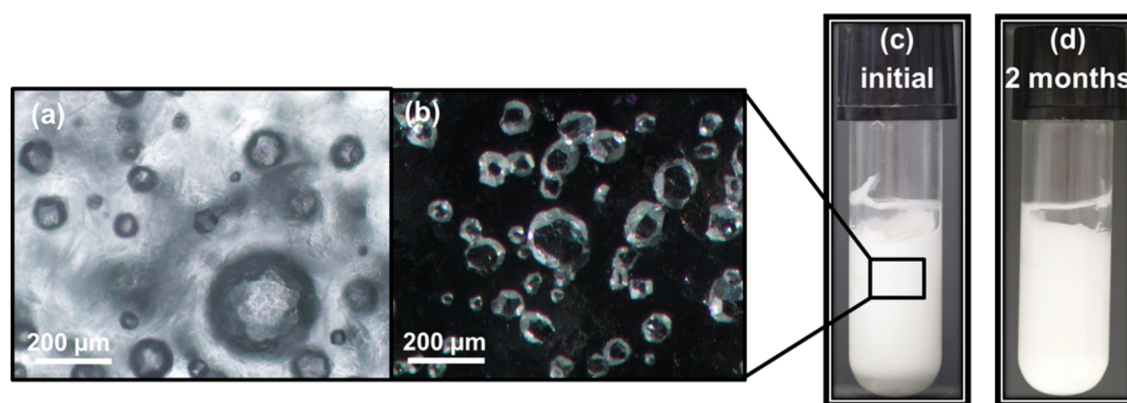


**Figure 6.** Micrographs of foams taken 1 min after foam formation from an oleogel containing 10 wt % C18OH, (a) observed under phase contrast and (b) polarized light. Foam bubbles are stabilized by the fatty alcohol particles, which adsorb to the bubble surface, leading to the formation of nonspherical bubbles with textured surfaces. Photographs of foams taken (c) 1 min and (d) 2 months after foam formation from an oleogel containing 10 wt % C18OH. The sample was stored at 20 °C.

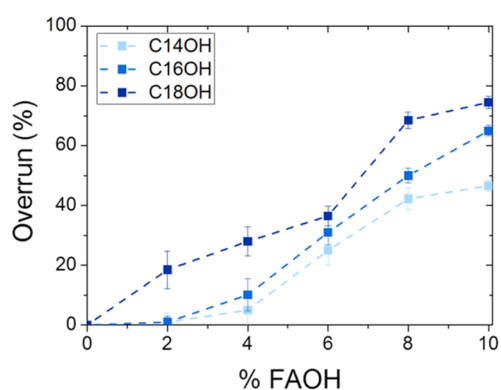


**Figure 7.** Foam overrun for samples produced from oleogels containing C14OH, C16OH, and C18OH as a function of FAOH concentration.

**Foam Stability as a Function of Temperature.** In the first part of our study, we demonstrated that the crystals leading to oleogel formation melted progressively over a wide range of temperatures from  $T_m$  onset to  $T_m$  offset (Figure 3). We studied the influence of crystal melting on foam stability by tuning the applied temperature. When foams were stored at only a few degrees above  $T_m$  onset, the sample flowed when the foam was turned upside down (Figure S11). Drainage occurred progressively as shown in Figure S12. By microscopy, we observed that the gel layer surrounding the bubbles became thinner and that mean bubble size increased in this case in comparison to foams kept below  $T_m$  onset. Moreover, bubbles adopted a more spherical shape. The crystals began to melt and the number of particles, which could stabilize the foam decreased. The quantity of crystals inside the bulk phase surrounding the bubbles decreased too, resulting in an increase in air diffusivity between bubbles.

When foams were stored at  $T > T_m$  offset, the bubbles vanished in few minutes, leading to the complete disappearance of the foam. Both the particles at the bubble surface as well as those located in the bulk phase of the oleogel melted, leading to a rapid disappearance of air bubbles (Figure 2b). This is illustrated in Movie 1 in which we can see the popping of bubbles during melting. Thus, these nonaqueous foams are thermoresponsive. As the melting of crystal particles was reversible, we studied the evolution of foam stability through

multiple temperature cycles (Figure 9). For foam produced from 10 wt % C18OH,  $T_m$  offset and  $T_c$  offset were 48.3 and 31.7 °C, respectively. At 20 °C ( $T < T_m$  onset), the foam was stable. However, when temperature was increased to 50 °C ( $T > T_m$  offset), the bulk phase between the bubbles transitioned from a gel to liquid state, leading to an onset in foam destabilization. By cooling the foam to 20 °C, the destabilization process was halted and the foam became stable again. The fatty alcohol was recrystallized at this temperature both in the bulk phase and around the bubbles. By again increasing the temperature to 50 °C, foam destabilization mechanisms were reactivated and the foam completely disappeared after 2 min. Thus, we showed that these nonaqueous foams are thermoresponsive systems for which the stability can be easily alternated between high and low by varying temperature.

**Photothermoresponsive Oil Foams.** The switchability between ultrastable and unstable foam depended solely on the temperature of the foam. Instead of heating the foam externally, the heat can be generated from internal heat sources incorporated in the foam matrix.<sup>13</sup> For example, carbon black particles (CBP) can absorb UV light and dissipate the absorbed energy as heat. The advantage of using light as a stimulus instead of temperature is that light can be precisely directed at a location of interest without physical contact with the sample.<sup>9</sup> For aqueous thermoresponsive foams stabilized by fatty acid self-assemblies, the presence of CBP inside foam films has been shown to induce rapid foam collapse upon UV or solar irradiation.<sup>13</sup> We extended this approach used for aqueous foams to develop photoresponsive non aqueous foams by incorporating CBP inside a C18OH foam sample. Foams produced from this mixture were ultrastable when stored below  $T_m$  onset and destabilized rapidly above  $T_m$  offset (Movie 2). CBP particles were trapped inside the matrix formed by the crystal particles between the bubbles (Figure S13). Under UV illumination from the top, foam destabilization was observed within minutes (Movies 3–5), resulting from the transition of the bulk phase from a gel to liquid state. In these samples, foam destabilization was accompanied by the disappearance of the bubbles from the foam as a result of enhanced gas diffusion due to a lack of stabilization at the oil–air interface caused by the melting of the FAOH crystals. The foam flowed when the quartz cell was inverted subsequent to UV light exposure (Figure 10). The same foam without CBP remained stable

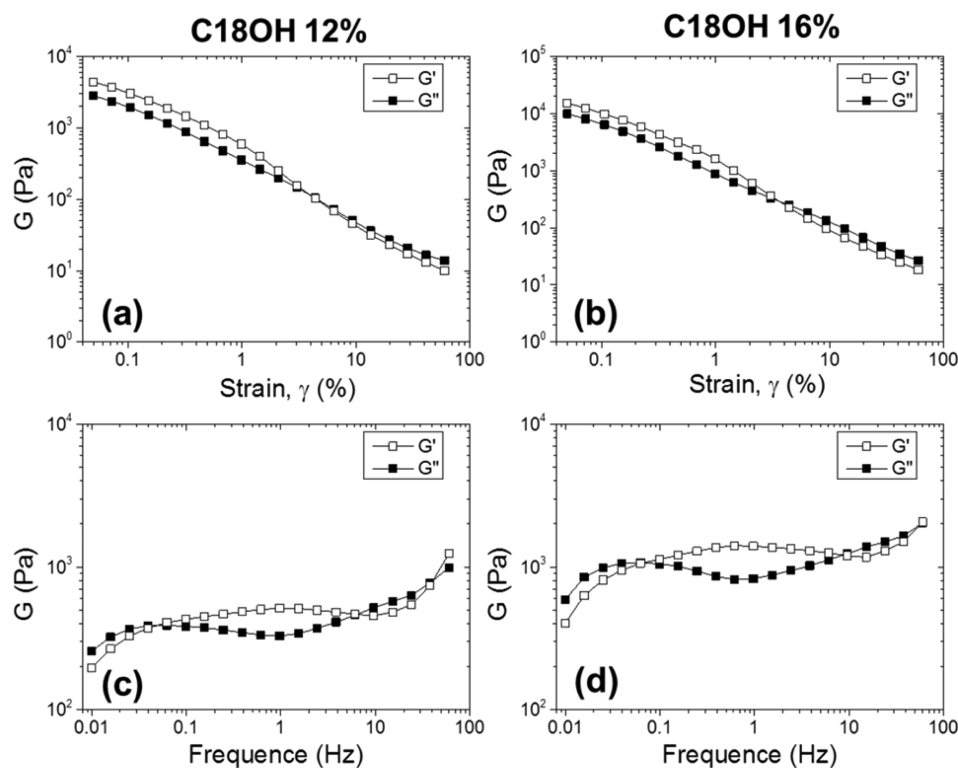


**Figure 8.** Frequency and strain amplitude sweep at 20 °C ( $T < T_m$  onset) for foams produced from oleogel containing C18OH at two concentrations: 12 wt % (a,c) and 16 wt % (b, d). Strain sweeps were performed at  $f = 1$  Hz, and frequency sweeps were performed at  $\gamma = 1\%$ .

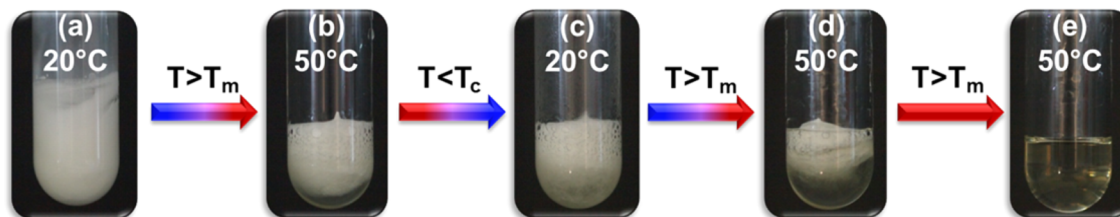


**Figure 9.** Photographs showing the stabilization/destabilization phenomena with temperature for a foam produced from oleogel containing 10 wt % C18OH, for which the offset of  $T_m$  and  $T_c$  were 48.3 and 31.7 °C, respectively. (a) Stable foam at 20 °C. (b) At 50 °C ( $T > T_{m \text{ offset}}$ ), foam destabilization started occurring in less than 1 min. (c) By decreasing the temperature back to  $T < T_c$  offset (20 °C), the foam became stable again. (d) Upon increasing the temperature to  $T > T_m$  offset for a second time, the onset of foam destabilization could again be observed in less than 1 min. (e) After 2 min at 50 °C, the foam was completely destroyed.

when exposed to the same conditions of UV illumination (Figure 10 and Movie 6). In these samples, no flow from the bulk phase or bubble disappearance was observed.

Under UV illumination, the CBPs absorbed the radiation and acted as photothermal heat generators to increase foam temperature above  $T_m$  onset. This causes crystal particles to melt progressively inside the foam, leading to destabilization. The foam collapse rate can be easily increased by increasing the CBP concentration from 0.01 to 1 wt % (Movies 3–5 and Figure S14). Moreover, foam destabilization could be instantaneously halted by removing the UV source. Thus, the oil foams presented here can be easily destabilized using UV radiation and this process can be activated and deactivated on demand.

## CONCLUSION

In conclusion, we introduced a novel approach to produce oil foams made from an oleogel based on simple components: fatty alcohol crystals dispersed in sunflower oil. We showed that the

oil foams could be easily produced by incorporating gas during the fatty alcohol crystallization process. The platelet crystals coat the air bubbles in the foam and mediate the gelification of the continuous phase, giving rise to ultrastable oil foams. The quantity of foam produced was directly linked to the quantity of crystal particles present to stabilize the air bubbles. We showed that foam stability was directly linked to hydrocarbon chain length and fatty alcohol concentration, both of which affect the formation and melting of the crystal particles. We demonstrated how one can adjust the temperature, fatty alcohol concentration, FAOH chain length, and extent of aeration to design oleogels with varying texture and viscoelasticity, ranging from those of a purely viscous liquid to that of a soft solid, and up to the one of a strong gel. The collapse of the foams could be induced rapidly upon heating due to the melting of the crystal particles surrounding the bubbles and in the continuous phase. The transition between crystal formation and melting was also found to be reversible leading to thermoresponsive nonaqueous foams. Up to our knowledge, this is the first study where the

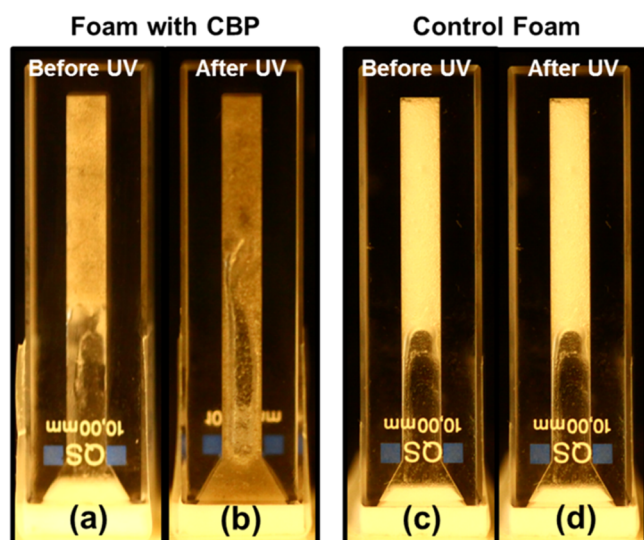


**Figure 10.** Photographs of foams produced from an oleogel containing 10 wt % C18OH and 0.01 wt % CBP (a) before illumination with UV light, and (b) 7 min after UV light illumination. Control foam made from an oleogel containing 10 wt % C18OH and 0 wt % CBP (c) before illumination with UV and (d) 7 min after illumination with UV light. CBP particles generate heat when exposed to UV radiation. Such particles can be used to tune the stability of oleogel foams via light stimulus. As seen in photographs (c) and (d), oleogel foams not containing CBP are not destabilized when irradiated with UV light.

effects of temperature on the rheology and phase transitions in oleogels are used in designing and characterizing strongly temperature-responsive nonaqueous foams. On this basis, we demonstrate a new class of photothermo-responsive oleogel foams, which can be destabilized by UV illumination. This approach to produce multiresponsive nonaqueous foams can be easily extended to food-grade oleogel systems based on fatty acids and monoglycerides.<sup>32,43,44</sup> These simple and inexpensive responsive oil foams based on oleogels could find applications in diverse industries such as cosmetic and food.

## EXPERIMENTAL SECTION

**Materials.** 1-Tetradecanol, 1-hexadecanol, and 1-octadecanol were purchased from Sigma-Aldrich. All the structuring agents were used without further purification. Sunflower oil was purchased from the local supermarket. Carbon black particles (CBP), Black Pearl880, were a gift from Cabot, Inc. (Billerica, MA).

**Oleogel Preparation.** Fatty alcohols (FAOH) were weighed in a sample tube into which sunflower oil was added to reach the desired concentration. Next, the mixture was heated for 5 min at 60–70 °C, which is sufficient to achieve full melting of all components. The transparent solution was vigorously vortexed and cooled to room temperature. The concentration of FAOH was varied from 1% (w/w) to 20% (w/w).

**Observations of Oleogels and Nonaqueous Foams Using Optical Microscopy.** The samples were visualized in an inverted microscope (Nikon Eclipse Ti-E, Tokyo, Japan) under phase-contrast with 20× or 40× objective lenses and an external light source for delivering light to the microscope through an optical cable. A Retiga Exi Blue camera (Q-Imaging, Vancouver, British Columbia) was used for image capture.

A SMZ 800 stereomicroscope (Nikon, Tokyo, Japan) mounted with a DS-Fi2 high-definition color camera, with a X1 Plan Apo objective and zoom capacities for a magnification range up to 6.8X has been used. The instrument is also equipped with an own oblique illuminator (OCC) for high contrast imaging as well as attachments for polarized light microscopy.

**Rheological Characterization of Oleogels and Nonaqueous Foams.** An Anton Paar MCR301 rheometer was used for rheological measurements. Experiments were performed using a plate–plate setup. The walls of the plates in contact with the samples were roughened to prevent slip. Temperature control was provided using a Peltier plate. The temperature ramp used for these experiments was 1 °C/min. An oscillatory frequency of 1 Hz and a strain of 1% were applied to measure the variation of the elastic modulus ( $G'$ ) and viscous modulus ( $G''$ ) with temperature to determine the temperature at which the transition between the oleogel state and liquid state occurred. Under the oscillatory mode, amplitude- and frequency-sweeps were performed to measure  $G'$  and  $G''$  as a function of the strain amplitude,  $\gamma$ , at constant frequency,  $f$ , and as a function of  $f$  at constant  $\gamma$ .

**Differential Scanning Calorimetry (DSC) of Oleogels.** Thermal properties of the oleogel were determined using a differential scanning calorimeter (TA Q100 instrument, New Castle, DE). All the samples were melted at 60–70 °C, and around 20 mg of the transparent solution was placed into a hermetically sealed aluminum pan for testing. An empty aluminum pan was used as a reference. DSC runs were carried out between 5 and 80 °C. The samples were scanned at a constant rate of 1 °C·min<sup>-1</sup> in the heating–cooling cycle. An isotherm of 5 min was performed at 80 °C before cooling and at 5 °C before heating. The transition temperatures were determined in duplicate for each sample. The peak melting temperatures ( $T_m$  onset and  $T_m$  offset), peak crystallization temperatures ( $T_c$  onset and  $T_c$  offset), enthalpy of melting, and enthalpy of crystallization were determined from the DSC curves using TA Instruments' Universal Analysis Software.

**Wide Angle X-ray Scattering (WAXS).** WAXS spectra were monitored by recording X-ray diffraction diagrams every 30 min on a Bruker D8 Discover diffractometer. Cu  $K\alpha_1$  radiation (Cu  $K\alpha_1 = 1.5405 \text{ \AA}$ ), produced in a sealed tube at 40 kV and 40 mA was selected and parallelized using a Göbel mirror optics system and collimated to produce a 500  $\mu\text{m}$  diameter beam. All samples were melted at 60–70 °C and placed in thin capillaries of 1.5 mm diameter which were then flame-sealed immediately. The temperature was varied from 5 to 50 °C and was controlled using a HFS 91-CAP platine (Linkam). In the case of the foam, the capillary was filled with foam at 25 °C and the WAXS spectrum was recorded at the same temperature. The averaged spectra were corrected for the solvent (sunflower oil) as well as the empty capillary tube.

**Foam Preparation and Characterization.** The oleogel was weighed out (7 g) in a glass container (2 cm internal diameter, 10 cm height). First, the gel was melted at 60 °C for 5 min. Then, the glass container was moved to an ice bath to induce crystallization during the homogenizing process. Foams were produced by homogenizing and aerating the oleogel in a single step with a whisk (1.8 cm diameter, 2.5 cm height) at a speed of 2000 rpm for 4 min immediately after placing the glass container in the ice bath (Figure S16). The overrun of the foam was calculated using<sup>45</sup>

$$\text{overrun (\%)} = \left[ \frac{V_t - V_0}{V_0} \right] \times 100$$

where  $V_t$  is the total volume of the foam and  $V_0$  is the initial liquid oil volume. The volume fraction of air corresponds to  $V_t - V_0$ , and the values are in the Supporting Information.

The change in foam volume with time was evaluated by visual inspection.

To produce photoresponsive foams, the desired amount of carbon black particles was added to the oleogel. The mixture was heated for 5 min at 60–70 °C. The oleogel was vortexed and then cooled to room temperature. In this case, foams were produced using two syringes. Hot oleogel was placed into one syringe, while the second syringe was filled with air. Both syringes were connected using a small segment of plastic tubing. Before use, the syringes were cooled in a freezer for at least 1 h so that rapid crystallization could occur during foam production. Agitation was achieved by pushing the plungers of both syringes back and forth to produce foams containing small bubbles. The foams were dispensed directly from the syringe into flat quartz

cells for testing with UV light. The quartz cells containing the foam were irradiated from the top using a 100 W UV lamp (OmniCure S1000, Efsen Engineering A/S, Denmark) operated at 75% intensity and equipped with a 320–500 nm band-pass filter. Foam evolution upon UV irradiation was recorded in digital video using a Canon EOS SD Camera with a 100 mm macro lens.

## ■ ASSOCIATED CONTENT

### 📄 Supporting Information

The Supporting Information is available free of charge on the ACS Publications website at DOI: [10.1021/acs.langmuir.5b03660](https://doi.org/10.1021/acs.langmuir.5b03660).

Part of the experimental section including DSC results, WAXS results, rheological results, and micrographs of oleogel foams (PDF)

Movie 1 showing the destruction of air bubbles inside an oleogel foam sample (8 wt % C18OH) when the temperature is increased above  $T_m$  offset (AVI)

Movie 2 showing destruction of air bubbles inside an oleogel foam (8 wt% C18OH) containing 0.1 wt % CBP when the temperature is increased above  $T_m$  offset (AVI)

Movie 3 showing light induced destabilization of oleogel foam (10 wt % C18OH) containing 0.01 wt % CBP (AVI)

Movie 4 showing light induced destabilization of oleogel foam (10 wt % C18OH) containing 0.1 wt % CBP (AVI)

Movie 5 showing light induced destabilization of oleogel foam (10 wt % C18OH) containing 1 wt % CBP (AVI)

Movie 6 showing that the oleogel foam (10 wt % C18OH) without CBP remains stable when irradiated with UV light (AVI)

## ■ AUTHOR INFORMATION

### Corresponding Authors

\*E-mail: [anne-laure.fameau@nantes.inra.fr](mailto:anne-laure.fameau@nantes.inra.fr) (A.-L.F.).

\*E-mail: [arnaud.saint-jalmes@univ-rennes1.fr](mailto:arnaud.saint-jalmes@univ-rennes1.fr) (A.S.-J.).

### Notes

The authors declare no competing financial interest.

## ■ ACKNOWLEDGMENTS

A.S.-J. and A.-L.F. acknowledge the COST (MP 1106) for support. INRA and Région Pays de la Loire are gratefully acknowledged for the Ph.D. grant of A.A. O.V. and S.L. gratefully acknowledge the U.S. Army Research Office (W911NF-15-1-0115) and partially the NSF Research Triangle MRSEC on Programmable Soft Matter (DMR-1121107) for financial support. A.S.-J. would like to thank Carole Sommier for her help during the rheological measurement.

## ■ REFERENCES

- (1) Weaire, D.; Hutzler, S. *The Physics of Foams*; Oxford University Press: Oxford, 1999.
- (2) Cantat, I.; Cohen-Addad, S.; Elias, F.; Graner, F.; Höhler, R.; Pitois, O. *Foams: structure and dynamics*; Oxford University Press: Oxford, 2013.
- (3) Lam, S.; Velikov, K. P.; Velev, O. D. Pickering stabilization of foams and emulsions with particles of biological origin. *Curr. Opin. Colloid Interface Sci.* **2014**, *19*, 490–500.
- (4) Fameau, A.-L.; Arnould, A.; Lehmann, M.; von Klitzing, R. Photoresponsive self-assemblies based on fatty acids. *Chem. Commun.* **2015**, *51*, 2907–2910.

- (5) Tang, C.; Xiao, E.; Sinko, P. J.; Szekeley, Z.; Prud'homme, R. K. Responsive Foams for Nanoparticle Delivery. *Colloids Surf., B* **2015**, *133*, 81–87.
- (6) Blanco, E.; Lam, S.; Smoukov, S. K.; Velikov, K. P.; Khan, S. A.; Velev, O. D. Stability and viscoelasticity of magneto-pickering foams. *Langmuir* **2013**, *29*, 10019–10027.
- (7) Lam, S.; Blanco, E.; Smoukov, S. K.; Velikov, K. P.; Velev, O. D. Magnetically responsive Pickering foams. *J. Am. Chem. Soc.* **2011**, *133*, 13856–13859.
- (8) Rio, E.; Drenckhan, W.; Salonen, A.; Langevin, D. Unusually stable liquid foams. *Adv. Colloid Interface Sci.* **2014**, *205*, 74–86.
- (9) Fameau, A.-L.; Carl, A.; Saint-Jalmes, A.; von Klitzing, R. Responsive Aqueous Foams. *ChemPhysChem* **2015**, *16*, 66–75.
- (10) Alargova, R. G.; Warhadpande, D. S.; Paunov, V. N.; Velev, O. D. Foam superstabilization by polymer microrods. *Langmuir* **2004**, *20*, 10371–10374.
- (11) Fujii, S.; Akiyama, K.; Nakayama, S.; Hamasaki, S.; Yusa, S.-i.; Nakamura, Y. pH-and temperature-responsive aqueous foams stabilized by hairy latex particles. *Soft Matter* **2015**, *11*, 572–579.
- (12) Zhu, Y.; Jiang, J.; Cui, Z.; Binks, B. P. Responsive aqueous foams stabilised by silica nanoparticles hydrophobised in situ with a switchable surfactant. *Soft Matter* **2014**, *10*, 9739–9745.
- (13) Fameau, A.-L.; Lam, S.; Velev, O. D. Multi-stimuli responsive foams combining particles and self-assembling fatty acids. *Chem. Sci.* **2013**, *4*, 3874–3881.
- (14) Fameau, A.-L.; Saint-Jalmes, A.; Cousin, F.; Houssou, B. H.; Novales, B.; Navailles, L.; Nallet, F.; Gaillard, C.; Boue, F.; Douliez, J.-P. Smart Foams: Switching Reversibly between Ultrastable and Unstable Foams. *Angew. Chem., Int. Ed.* **2011**, *50*, 8264–8269.
- (15) Chevallier, E.; Monteux, C.; Lequeux, F.; Tribet, C. Photofoams: Remote Control of Foam Destabilization by Exposure to Light Using an Azobenzene Surfactant. *Langmuir* **2012**, *28*, 2308–2312.
- (16) Zhang, L.; Mikhailovskaya, A.; Yazhgur, P.; Muller, F.; Cousin, F.; Langevin, D.; Wang, N.; Salonen, A. Precipitating Sodium Dodecyl Sulfate to Create Ultrastable and Stimulable Foams. *Angew. Chem.* **2015**, *127*, 9669–9672.
- (17) Friberg, S. E. Foams from non-aqueous systems. *Curr. Opin. Colloid Interface Sci.* **2010**, *15*, 359–364.
- (18) Bergeron, V.; Hanssen, J. E.; Shoghl, F. Thin-film forces in hydrocarbon foam films and their application to gas-blocking foams in enhanced oil recovery. *Colloids Surf., A* **1997**, *123*, 609–622.
- (19) Binks, B.; Davies, C.; Fletcher, P.; Sharp, E. Non-aqueous foams in lubricating oil systems. *Colloids Surf., A* **2010**, *360*, 198–204.
- (20) Friberg, S. E.; Solans, C. Surfactant association structures and the stability of emulsions and foams. *Langmuir* **1986**, *2*, 121–126.
- (21) Friberg, S. E.; Wohn, C. S.; Greene, B.; Van Gilder, R. A nonaqueous foam with excellent stability. *J. Colloid Interface Sci.* **1984**, *101*, 593–595.
- (22) Binks, B. P. Particles as surfactants—similarities and differences. *Curr. Opin. Colloid Interface Sci.* **2002**, *7*, 21–41.
- (23) Binks, B. P.; Rocher, A. Stabilisation of liquid–air surfaces by particles of low surface energy. *Phys. Chem. Chem. Phys.* **2010**, *12*, 9169–9171.
- (24) Binks, B. P.; Rocher, A.; Kirkland, M. Oil foams stabilised solely by particles. *Soft Matter* **2011**, *7*, 1800–1808.
- (25) Murakami, R.; Bismarck, A. Particle-Stabilized Materials: Dry Oils and (Polymerized) Non-Aqueous Foams. *Adv. Funct. Mater.* **2010**, *20*, 732–737.
- (26) Binks, B. P.; Tyowua, A. T. Influence of the degree of fluorination on the behaviour of silica particles at air–oil surfaces. *Soft Matter* **2013**, *9*, 834–845.
- (27) Kunieda, H.; Shrestha, L. K.; Acharya, D. P.; Kato, H.; Takase, Y.; Gutiérrez, J. M. Super-Stable Nonaqueous Foams in Diglycerol Fatty Acid Esters—Non Polar Oil Systems. *J. Dispersion Sci. Technol.* **2007**, *28*, 133–142.
- (28) Shrestha, L. K.; Aramaki, K.; Kato, H.; Takase, Y.; Kunieda, H. Foaming properties of monoglycerol fatty acid esters in nonpolar oil systems. *Langmuir* **2006**, *22*, 8337–8345.

(29) Shrestha, L. K.; Shrestha, R. G.; Sharma, S. C.; Aramaki, K. Stabilization of nonaqueous foam with lamellar liquid crystal particles in diglycerol monolaurate/olive oil system. *J. Colloid Interface Sci.* **2008**, *328*, 172–179.

(30) Shrestha, R. G.; Shrestha, L. K.; Solans, C.; Gonzalez, C.; Aramaki, K. Nonaqueous foam with outstanding stability in diglycerol monomyristate/olive oil system. *Colloids Surf, A* **2010**, *353*, 157–165.

(31) Brun, M.; Delample, M.; Harte, E.; Lecomte, S.; Leal-Calderon, F. Stabilization of air bubbles in oil by surfactant crystals: A route to produce air-in-oil foams and air-in-oil-in-water emulsions. *Food Res. Int.* **2015**, *67*, 366–375.

(32) Perneti, M.; van Malssen, K. F.; Flöter, E.; Bot, A. Structuring of edible oils by alternatives to crystalline fat. *Curr. Opin. Colloid Interface Sci.* **2007**, *12*, 221–231.

(33) Co, E. D.; Marangoni, A. G. Organogels: an alternative edible oil-structuring method. *J. Am. Oil Chem. Soc.* **2012**, *89*, 749–780.

(34) Dassanayake, L. S. K.; Kodali, D. R.; Ueno, S. Formation of oleogels based on edible lipid materials. *Curr. Opin. Colloid Interface Sci.* **2011**, *16*, 432–439.

(35) Lupi, F.; Gabriele, D.; Greco, V.; Baldino, N.; Seta, L.; de Cindio, B. A rheological characterisation of an olive oil/fatty alcohols organogel. *Food Res. Int.* **2013**, *51*, 510–517.

(36) Rogers, M. A. Novel structuring strategies for unsaturated fats—meeting the zero-trans, zero-saturated fat challenge: a review. *Food Res. Int.* **2009**, *42*, 747–753.

(37) Gandolfo, F. G.; Bot, A.; Flöter, E. Structuring of edible oils by long-chain FA, fatty alcohols, and their mixtures. *J. Am. Oil Chem. Soc.* **2004**, *81*, 1–6.

(38) Schaink, H.; Van Malssen, K.; Morgado-Alves, S.; Kalnin, D.; Van der Linden, E. Crystal network for edible oil organogels: possibilities and limitations of the fatty acid and fatty alcohol systems. *Food Res. Int.* **2007**, *40*, 1185–1193.

(39) Daniel, J.; Rajasekharan, R. Organogelation of plant oils and hydrocarbons by long-chain saturated FA, fatty alcohols, wax esters, and dicarboxylic acids. *J. Am. Oil Chem. Soc.* **2003**, *80*, 417–421.

(40) Hughes, N. E.; Marangoni, A. G.; Wright, A. J.; Rogers, M. A.; Rush, J. W. Potential food applications of edible oil organogels. *Trends Food Sci. Technol.* **2009**, *20*, 470–480.

(41) Subramaniam, A. B.; Mejean, C.; Abkarian, M.; Stone, H. A. Microstructure, morphology, and lifetime of armored bubbles exposed to surfactants. *Langmuir* **2006**, *22*, 5986–5990.

(42) Gopal, A. D.; Durian, D. J. *Phys. Rev. Lett.* **2003**, *91*, 188303.

(43) Nikiforidis, C. V.; Gilbert, E. P.; Scholten, E. Organogel formation via supramolecular assembly of oleic acid and sodium oleate. *RSC Adv.* **2015**, *5*, 47466–47475.

(44) Mezzenga, R.; Ulrich, S. *Langmuir* **2010**, *26*, 16658–16661.

(45) Prud'homme, R. K.; Khan, S. A., Eds. *Foams- Theory, measurements and applications*; Marcel Dekker: New York, 1996.